Surface reconstructions on bare and hydrogenated β-Ga$_2$O$_3$ surfaces: Implications for growth

Mengen Wang ⬤, Sai Mu, and Chris G. Van de Walle ⬤[*]

Materials Department, University of California, Santa Barbara, California 93106-5050, USA

Hydrogen is present during the growth of β-Ga$_2$O$_3$ using chemical vapor deposition techniques. A detailed understanding of hydrogen-related surface reconstructions is therefore essential for controlling the material properties. We use density functional theory to explore the adsorption of hydrogen, gallium, and oxygen adatoms on the Ga$_2$O$_3$(010) and Ga$_2$O$_3$(110) surfaces and generate a surface phase diagram, which shows surface reconstructions as a function of Ga and H chemical potentials. We find that the reconstructions on (110) and (010) surfaces are similar, due to the similarity in bonding. In the absence of hydrogen we find that the ideal unreconstructed surface is low in energy but that reconstructions with Ga and O adatoms can be favorable under more Ga-rich conditions. We question whether such "bare" surfaces can be experimentally observed, since hydrogen-related reconstructions are favored even at very low hydrogen pressures (consistent with residual gas pressures in ultrahigh-vacuum systems). Under more H-rich conditions, multiple hydrogen-containing reconstructions are found, with H adsorption being more stable under O-rich conditions. We find that the electron counting rule is valuable for assessing the stability of surface reconstructions. Knowledge of surface reconstructions and of the stability of hydrogen on the surface will help tailor growth conditions to achieve optimal layer quality.

I. INTRODUCTION

Monoclinic β-Ga$_2$O$_3$ is a wide-band-gap (4.8 eV) semiconductor that can be *n*-type doped, making it a promising material for power electronics based on Schottky-barrier diodes [1] or field-effect transistors [2,3]. Hydrogen distinctly impacts the properties of the material. In the bulk, hydrogen incorporation can affect the conductivity of Ga$_2$O$_3$: It acts as a shallow donor either in interstitial (H$_i$) or substitutional sites (H$_O$) [4]. Hydrogen can also passivate acceptors by bonding to a nearby O atom; it has been found that hydrogen annealing neutralizes substitutional Mg (Mg$_{Ga}$) by forming a Mg$_{Ga}$–H complex [5]. Hydrogen can also form complexes with gallium vacancies (V_{Ga}): Hydrogenated Ga vacancies (V_{Ga}–H) have lower formation energies than isolated V_{Ga} and are partially passivated [6,7]. In addition to affecting the bulk properties, the presence of hydrogen on the surface may also modify the growth mode. It is therefore essential to develop a detailed understanding of the behavior of hydrogen on the Ga$_2$O$_3$ surface.

Hydrogen is present in many growth techniques, particularly chemical vapor deposition. Metal-organic chemical vapor deposition (MOCVD) is widely used for growth of Ga$_2$O$_3$, with Ga(CH$_3$)$_3$ or Ga(C$_2$H$_5$)$_3$ as Ga precursors and H$_2$O or O$_2$ as O precursors [8,9]. In hydride (or halide) vapor phase epitaxy, HCl is used to react with Ga to produce GaCl, and H$_2$O is often used as the oxygen precursor, both of which can introduce H during the growth [10–12]. Using chemical vapor deposition techniques, β-Ga$_2$O$_3$ is usually grown at temperatures above 700 °C, and a high oxygen-to-metal ratio

is desired to achieve complete combustion of hydrocarbons and prevent etching of the Ga$_2$O$_3$ surface [13,14].

When H$_2$O is used as the O precursor, dissociation of water results in the generation of H$_2$ and becomes the major source for hydrogen [9,10,15]. Switching between H$_2$O and O$_2$ as the O precursor has allowed the effect of hydrogen to be studied. Introducing water vapor during MOCVD growth of Ga$_2$O$_3$(010) leads to higher surface roughness than using pure O$_2$ as the precursor, mainly due to the growth of {110} facets, indicating that H affects the relative stability of different Ga$_2$O$_3$ surface orientations [9].

A detailed understanding of surface reconstructions and of the adsorption of H during epitaxial growth is essential for controlling material properties. Some density functional theory (DFT) studies have already been performed for H adsorption on the ideal (unreconstructed) Ga$_2$O$_3$(100) surface [16,17], H on the Ga$_2$O$_3$(100) surface with O vacancies, and H on the bare (110) surface [18]. The formation of O vacancies on Ga$_2$O$_3$ surfaces has also been calculated [19].

Here we present systematic DFT calculations for surface reconstructions on both bare and hydrogenated (010) surfaces; this is the most widely used surface for epitaxial growth of Ga$_2$O$_3$, due to the growth rate being higher than for (001) or (100) surfaces and the fact that the symmetry of the (010) surface prevents the formation of planar defects such as stacking faults [20]. We comprehensively explore surface structures, which in addition to hydrogen may involve coadsorption of Ga and O. We also study the H adsorption on the (110) surface and the role of H in stabilizing the (110) surface. We examine the structure and energetics of these reconstructed surfaces, using the electron counting rule to elucidate the stability of different reconstructions.

We present the results in the form of a surface phase diagram as a function of H, Ga, and O chemical potentials, thus
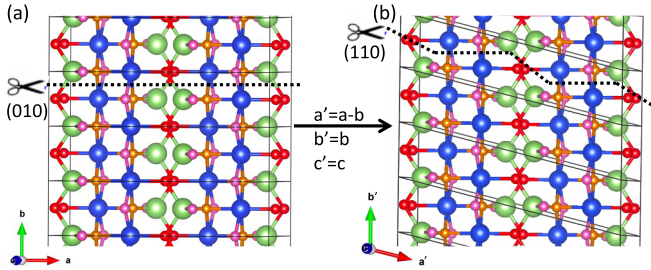
---

*vandewalle@mrl.ucsb.edu

FIG. 1. Layer stacking used to study (a) (010) and (b) (110) surfaces of Ga$_2$O$_3$.

accounting for realistic growth conditions. For bare surfaces, in the absence of hydrogen, we find that the ideal unreconstructed surface (which obeys electron counting) is favored, except under more Ga-rich conditions where reconstructions with Ga and O adatoms prevail. When hydrogen is present (even at the very low pressures found in ultrahigh-vacuum systems), hydrogen-related reconstructions are favored. Hydrogen easily adsorbs on the surface, particularly under O-rich (Ga-poor) conditions, due to the formation of strong O–H bonds. A Ga+2O+H reconstruction involving one Ga atom, two O atoms, and one H atom is favorable over a large range of conditions. For the (110) surface we find that the Ga+2O+H reconstruction is more favorable than on the (010) surface, which may help explain formation of {110} facets during growth under more H-rich conditions.

II. COMPUTATIONAL METHODS

Our DFT calculations are performed using the projector augmented-wave method implemented in the Vienna

ab initio simulation package (VASP) [21,22]. The Perdew-Burke-Ernzerhof (PBE) functional [23] is used. Ga 3d electrons are explicitly treated as valence electrons. The energy cutoff is set to 520 eV. The computed lattice constants of Ga$_2$O$_3$ are $a = 12.47$ Å, $b = 3.09$ Å, $c = 5.88$ Å, and $\beta = 103.68°$, in reasonable agreement with experimental values [24] ($a = 12.21$ Å, $b = 3.04$ Å, $c = 5.82$ Å, and $\beta = 103.82°$).

Each conventional unit cell of β-Ga$_2$O$_3$ contains two atomic layers in the [010] direction, which is usually called a "double layer." We study the Ga$_2$O$_3$(010) surface by stacking five double layers along the [010] direction, forming a $1 \times 5 \times 1$ supercell as illustrated in Fig. 1(a). Similarly, in order to study the (110) surface, we stack five layers of the conventional cell in the [110] direction [Fig. 1(b)]. The vacuum thickness is ∼19 Å, and a $2 \times 1 \times 4$ **k**-point grid is used to sample the Brillouin zone. The inversion symmetry of the slabs allows identical reconstructions on both sides, which enables the properties of a single surface to be extracted. Atoms in the central double layer are kept fixed, while atoms in the two double layers near the surfaces of the slab and adatoms are allowed to relax during the structural optimization until forces are smaller than 0.01 eV/Å.

Figure 2(a) illustrates the two types of Ga atoms in β-Ga$_2$O$_3$: Ga on the tetrahedral site (Ga$_{tetra}$ in green) and Ga on the octahedral site (Ga$_{octa}$ in blue). Ga$_{tetra}$ and Ga$_{octa}$ are sometimes also labeled Ga$_I$ and Ga$_{II}$. Figure 2(a) also illustrates the three types of O atoms: O$_I$ (magenta) is threefold coordinated to two Ga$_{octa}$ atoms and one Ga$_{tetra}$ atom, O$_{II}$ (red) is threefold coordinated to two Ga$_{tetra}$ atoms and one Ga$_{octa}$ atom, and O$_{III}$ (orange) is fourfold coordinated to three Ga$_{octa}$ atoms and one Ga$_{tetra}$ atom. The top view of the (010) surface
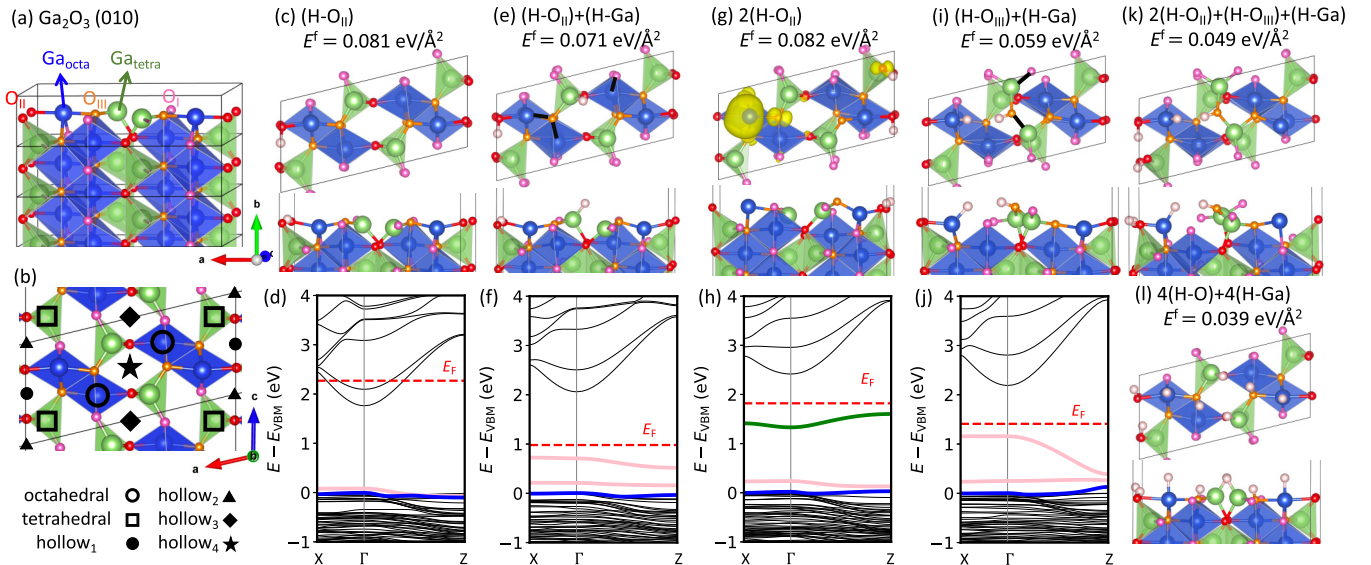

FIG. 2. Side (a) and top (b) view of the ideal β-Ga$_2$O$_3$(010) surface. The adsorption sites we explored are labeled in (b), consistent with Ref. [25]. Color code: Ga$_{tetra}$ (green), Ga$_{octa}$ (blue), O$_I$ (magenta), O$_{II}$ (red), O$_{III}$ (orange), and H (white). Structure of the Ga$_2$O$_3$(010) surface with (c) (H–O$_{II}$), (e) (H–O$_{II}$)+(H–Ga), (g) 2(H–O$_{II}$), (i) (H–O$_{III}$)+(H–Ga), (k) 2(H–O$_{II}$)+(H–O$_{III}$)+(H–Ga), and (l) 4(H–O)+4(H–Ga). Atoms are presented in a polyhedral style, except for atoms in the top layer, which are presented in a ball-and-stick style. The quoted formation energies E^f are for $\Delta\mu_H = 0$. The corresponding band structures for the surfaces are shown in the second row of panels: (d) (H–O$_{II}$), (f) (H–O$_{II}$)+(H–Ga), (h) 2(H–O$_{II}$), and (j) (H–O$_{III}$)+(H–Ga). The blue band is the highest valence band, green and pink bands are surface states, and the red dashed line is the Fermi level (E_F). The yellow charge density isosurface superimposed on the atomic structures in (g) is for the green band.

[Fig. 2(b)] illustrates possible adsorption sites for Ga and O adatoms.

The formation energy E^f of a reconstructed surface is defined as

$$E^f = \tfrac{1}{2}(E_{tot} - E_{bulk} - 2\mu_i n_i)/A_{surface}. \quad (1)$$

E_{tot} is the total energy of the slab with reconstructed surface. The reference energy E_{bulk} is the energy of a corresponding volume of bulk Ga_2O_3, and E^f is normalized by the area of the surface unit cell; $A_{surface}$ is 71.26 Å^2 for (010) and 73.54 Å^2 for (110). n_i is the number of adsorbed adatoms on a single surface, and μ_i is the chemical potential of species i (H, Ga, or O). $\Delta\mu_i$ is the deviation of the chemical potential from the reference state, i.e., $\mu_i = \mu_{i,ref} + \Delta\mu_i$. $\mu_{i,ref}$ is the energy of atomic species i calculated for the elemental phase (bulk Ga, O_2 molecule, or H_2 molecule). Assuming thermodynamic equilibrium, $\Delta\mu_{Ga}$ and $\Delta\mu_O$ are related by

$$2\Delta\mu_{Ga} + 3\Delta\mu_O = \Delta H^f(Ga_2O_3), \quad (2)$$

where $\Delta H^f(Ga_2O_3) = -9.22$ eV is the calculated formation enthalpy of Ga_2O_3. Under the constraints of $\Delta\mu_i < 0$, the range of $\Delta\mu_{Ga}$ is -4.61 eV $< \Delta\mu_{Ga} < 0$ eV.

Equation (1) also includes finite-temperature effects. The strongest energy dependence arises from the chemical potentials of gaseous elements; for example, the temperature and pressure dependence of $\Delta\mu_H$ is expressed as

$$\Delta\mu_H = \frac{1}{2}kT\left\{\ln\left[\frac{p}{kT}\left(\frac{h^2}{2\pi mkT}\right)^{\frac{3}{2}}\right] - \ln Z_{rot} - \ln Z_{vib}\right\}, \quad (3)$$

where k is the Boltzmann constant, T is the temperature, p is H_2 pressure, and Z_{rot} and Z_{vib} are the rotational and vibrational partition functions of the H_2 molecule [26]. A weaker temperature dependence arises from surface contributions to vibrational energy and entropy. Previous studies have shown that these result in only minor changes in the free energy [27]. We therefore do not include this effect in the formation energies.

The calculated band gap of bulk Ga_2O_3 using the PBE functional is 2.0 eV. The band gap of the (010) slab is 2.24 eV, which is larger than the bulk Ga_2O_3 band gap due to quantum confinement. In order to test the accuracy of structures and formation energies obtained with PBE, we performed tests using the hybrid functional of Heyd, Scuseria, and Ernzerhof (HSE06) [28,29] with a mixing parameter of $\alpha = 0.32$, which yields very good results for the electronic structure of Ga_2O_3 [30]. A comparison of HSE and PBE energies will be reported in Sec. III B.

III. RESULTS AND DISCUSSION

A. Hydrogen adsorption on the ideal β-Ga$_2$O$_3$(010) surface

We first examine how hydrogen interacts with the ideal (unreconstructed) β-Ga$_2$O$_3$(010) surface (Fig. 2). When a single H is added, it prefers to bond to an O_{II} atom [Fig. 2(c)], with an adsorption energy equal to 0.42 eV. We define

the adsorption energy as the energy difference between the hydrogen-adsorbed surface and the ideal (unreconstructed but relaxed) surface, assuming $\Delta\mu_H = 0$, with a sign such that a positive value indicates stable adsorption. A value of 0.42 eV may seem surprisingly low for O–H, which is expected to have a high binding energy. The low value can be explained by the fact that the ideal β-Ga$_2$O$_3$(010) surface obeys the electron counting rule [31]. This rule says that anion dangling bonds (DBs) prefer to be occupied because they have states in the valence band or in the lower part of the gap, and cation DBs prefer to be unoccupied because their states are in the conduction band or in the upper part of the band gap. We can calculate the total number of electrons on the ideal, unreconstructed Ga_2O_3(010) surface by counting the electrons provided by the broken bonds in Fig. 2(a): The four Ga atoms provide $2 \times (3/4) + 4 \times (1/2) = 7/2$ electrons, and the six O atoms provide $2 \times (5/4) + 2 \times (3/2) + 2 \times (3/2) = 17/2$ electrons. The total of 12 electrons is exactly right to fill all the O DBs on the surface and leave all Ga DBs empty [25]. The pink band in Fig. 2(d) is a filled surface state that originates from the O_{II} DBs. Since all O DBs are already fully occupied, when a H atom is added the O_{II}–H bond cannot accommodate the electron contributed by H; this electron needs to go into the lowest unoccupied state, which corresponds to the conduction band [Fig. 2(d)], thus raising the energy.

Bonding is more favorable when *two* H adatoms are adsorbed on the surface: Now one H is bonded to an O_{II}, and the other H is bonded to a Ga_{tetra}, with a resulting adsorption energy of 1.19 eV [Fig. 2(e)]. The two electrons contributed by the H adatoms go into the Ga–H bond, and the corresponding bonding state merges to the valence band. The two surface states in the gap [pink bands in Fig. 2(f)] originate from surface O atoms and are close to the valence band maximum (VBM).

Attempting to bind both of the H atoms to O atoms [Fig. 2(g)] results in a less stable arrangement with an adsorption energy of only 0.36 eV. The two electrons now go into a Ga DB, which has a surface state [green band in Fig. 2(h)] that is significantly higher in energy than the (O-related) surface states in Fig. 2(f). Building on this pattern, we can keep adding pairs of H atoms, leading to the 4(H–O)+4(H–Ga) [Fig. 2(l)] surfaces. At $T = 0$, the surface with eight H adatoms has the lowest formation energy and largest adsorption energy (3.43 eV). Here four H adatoms are bonded to the four surface Ga atoms, and the other four H adatoms are bonded to two surface O_{II} atoms and two surface O_{III} atoms.

We actually found, for the surface with two H adatoms, that we can lower the surface energy by allowing for more extensive rebonding, leading to an adsorption energy of 2.00 eV [Fig. 2(i)]. This requires breaking three Ga_{octa}–O bonds (two Ga_{octa}–O_{III} bonds and one Ga_{octa}–O_I bond); these bonds are indicated by three thick black lines in Fig. 2(e). Four new bonds are formed: Ga_{tetra}–O_{III}, Ga_{tetra}–O_I, Ga_{octa}–H, and O_{III}–H. The new Ga_{tetra}–O_{III} and Ga_{tetra}–O_I bonds are labeled by two thick black lines in Fig. 2(i). We can understand the stability based on electron counting. Each of the three broken bonds contributes two electrons. Taking the two electrons from the H adatoms into account, there are $2 + 3 \times 2 = 8$ electrons that go to the four new bonds, with bonding states that all merge into the valence band [Fig. 2(j)]. The two
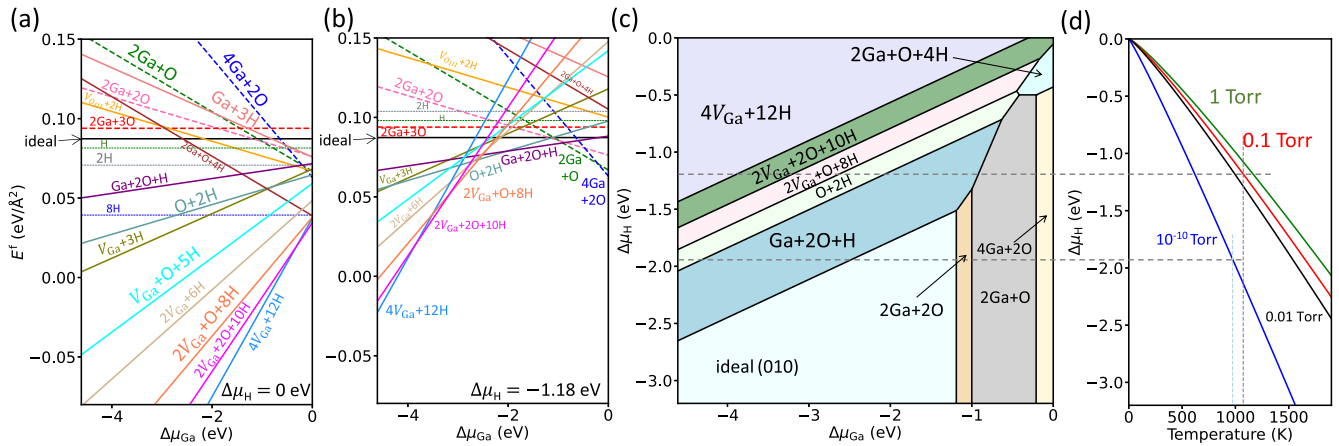
FIG. 3. Formation energies E^f (in eV/Å^2) for various (010) surface reconstructions as a function of the Ga chemical potential when (a) $\Delta\mu_H = 0$ eV and (b) $\Delta\mu_H = -1.18$ eV. (c) Phase diagram of the Ga$_2$O$_3$(010) surface as a function of $\Delta\mu_{Ga}$ and $\Delta\mu_H$. (d) $\Delta\mu_H$ as a function of temperature for H$_2$ pressures of 1, 0.1, and 0.01 Torr. The dashed line at $\Delta\mu_H = -1.18$ eV is representative of conditions in MOCVD growth; the dashed line at $\Delta\mu_H = -1.92$ eV is representative of conditions in ultrahigh vacuum.

surface states in the lower part of the gap [pink bands in Fig. 2(j)] again originate from surface O atoms. The rebonding on the surface [Fig. 2(b)] breaks two Ga$_{octa}$–O bonds and allows the formation of two Ga$_{tetra}$–O bonds. Since Ga$_{tetra}$–O bonds are stronger than Ga$_{octa}$–O bonds, the rebonding lowers the formation energy. We found that breaking and re-forming new Ga–O bonds can also result in lower formation energies for higher H coverages. For example, rebonding on the surface with four H atoms [Fig. 2(k)] occurs similarly to rebonding on the surface with two H atoms [Fig. 2(i)]. For the surface with eight H atoms [Fig. 2(l)], rebonding does not lower the surface energy.

These rebonded structures may not necessarily be experimentally observable, since the required bond breaking may not be able to occur in a concerted fashion either during growth or during postgrowth hydrogenation. We also note that the rebonding requires a chain of new bonds to form along the [001] direction. However, the stability of these rebonded structures indicates that surface reconstructions that offer opportunities for forming new Ga–O bonds due to the presence of additional Ga or O atoms could be very favorable; this will be addressed in Secs. III B and III C.

Formation energies of H adsorption on ideal β-Ga$_2$O$_3$(010) surfaces at $T = 0$ are included in Fig. 3(a). Effects of finite temperature can be taken into account by changing the chemical potential of hydrogen. In Fig. 3(d) we show how $\Delta\mu_H$ changes as the temperature is increased. As an example, at $T = 800$ °C and $p = 0.1$ Torr, $\Delta\mu_H$ is decreased by 1.18 eV compared with $T = 0$. We note that $T = 800$ °C and $p = 0.1$ Torr correspond to typical growth conditions in MOCVD [13]. The lowering of $\Delta\mu_H$ significantly increases the formation energies of H-adsorbed surfaces, particularly those with high hydrogen coverage, as seen in Fig. 3(b). Among the surfaces with pure H adsorption discussed so far, the surface with eight H atoms is lowest in energy at $T = 0$, but its energy shoots up at high temperature. Figure 3 shows that structures with hydrogen adsorbed on the ideal stoichiometric structure are never the lowest-energy structure once deviations from

stoichiometry are allowed (as will evidently be the case during growth). Such structures are discussed in the next section.

B. Reconstructions on bare surfaces

We will now examine reconstructions that allow for changing the surface stoichiometry. We explored various coverages of Ga and O that span the range from Ga-rich conditions ($\Delta\mu_{Ga} = 0$ eV) to O-rich conditions ($\Delta\mu_{Ga} = -4.61$ eV). As each atomic layer of Ga$_2$O$_3$ in the [010] orientation contains four Ga atoms and six O atoms, we consider between zero and four Ga adatoms and between zero and six O adatoms. For each specific coverage, we explored all adsorption sites illustrated in Fig. 2(b) as initial positions for Ga and O to determine the most stable configuration. This investigation also includes structures that could be considered to contain Ga and O vacancies. For example, the reconstruction with a Ga vacancy (V_{Ga}) is equivalent to the adsorption of three Ga and six O adatoms. For these vacancy reconstructions, we also explore Ga and/or O sites that differ from the bulk positions, including sites with different coordinations, and determine the most stable configuration.

In Fig. 3 we display results for reconstructions that have relatively low formation energies in some part of the phase space spanned by $\Delta\mu_{Ga}$, either under very H-rich conditions, $\Delta\mu_H = 0$ [Fig. 3(a)], relevant for exposure to hydrogen at relatively low temperatures, or under conditions more relevant for the presence of H during growth, $\Delta\mu_H = -1.18$ eV [Fig. 3(b)]. As we can see, the stability of various reconstructions sensitively depends on both $\Delta\mu_{Ga}$ and $\Delta\mu_H$; it is thus useful to present the results in the form of a surface phase diagram [Fig. 3(c)] that indicates which reconstruction is most stable for each combination of Ga and H chemical potentials.

Looking along a horizontal line near the bottom of the phase diagram, we identify reconstructions that are stable in the absence of hydrogen. Under Ga-rich conditions, we find the surfaces with 4Ga+2O [Fig. 4(a)], 2Ga+O [Fig. 4(b)], and 2Ga+2O [Fig. 4(c)] reconstructions to be stable. Under less

(a) 4Ga+2O
$E^f = 0.063$ eV/Å^2

(b) 2Ga+O
$E^f = 0.067$ eV/Å^2

(c) 2Ga+2O
$E^f = 0.076$ eV/Å^2

(d)
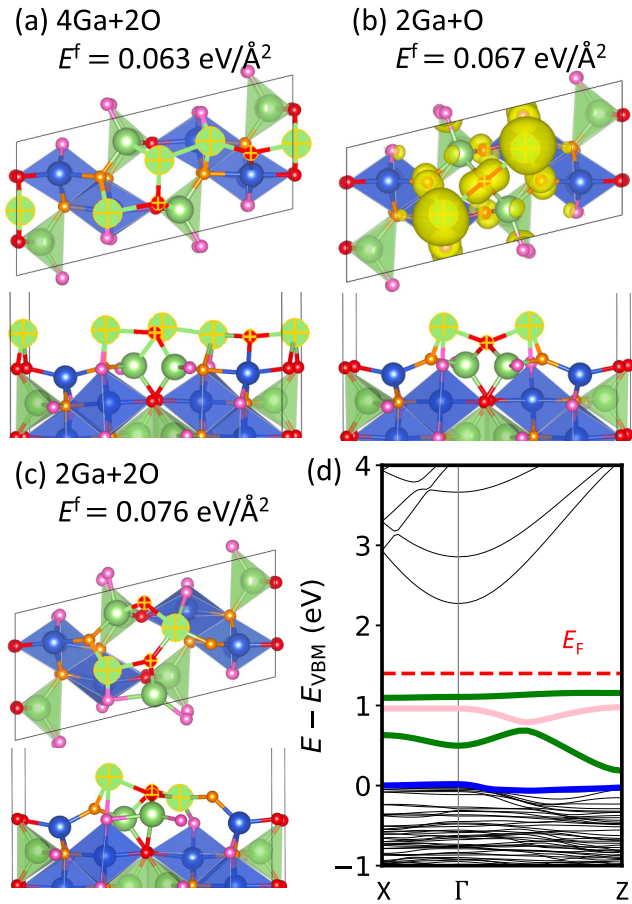
FIG. 4. Structures of Ga$_2$O$_3$(010) surfaces with (a) 4Ga+2O, (b) 2Ga+O, and (c) 2Ga+2O. The quoted formation energies E^f are for $\Delta\mu_{Ga} = \Delta\mu_H = 0$. (d) Band structure of the 2Ga+O surface displayed in (b). The yellow charge density isosurface superimposed on the atomic structures in (b) is for the green bands.

Ga-rich conditions, we find the ideal (bare unreconstructed) surface to be most stable. We note that, as seen in Figs. 3(a) and 3(b), the complexity of the Ga$_2$O$_3$ structure leads to other surface reconstructions having energies that are only slightly higher than the most stable structure; this indicates that, even for a fixed set of chemical potentials, more than one reconstruction could potentially be observed at finite temperature.

We explore the origins of the stability of specific reconstructions by invoking the electron counting rule. Each Ga, O, or H adatom contributes three electrons, six electrons, or one electron to the surface. On the ideal surface, all O DBs are filled; bonds formed with surface O therefore do not need any additional electrons, and electrons introduced by adatoms will therefore go to bonds formed among adatoms, to bonds formed between surface Ga atoms and adatoms, or into DBs of O adatoms, Ga adatoms, or surface Ga. When vacancies are created, H adatoms can bind to the exposed DBs. Based on the electron counting rule, the reconstructed surface tends to maximize the number of bonds formed on the surface and minimize the number of electrons localized on Ga DBs. The total number of electrons that will be associated with Ga atoms (n_e) is counted by

$$n_e = 3n_{Ga} + 6n_O + n_H - 2n_{bonds} - 2n_{ODB}. \qquad (4)$$

n_{ODB} is the number of occupied dangling bonds of O adatoms, and n_{bonds} is the number of Ga–O, Ga–H, and O–H bonds. We do not count Ga–Ga bonds since these may give rise to levels in the band gap. O–H or O–Ga bonds that are formed with O atoms present on the unreconstructed surface are not included in n_{bonds}; this is because DBs of these surface O atoms are fully occupied and cannot accommodate any electrons from adatoms.

As an example, let us look at the surface with 2Ga+O [Fig. 4(b)]. Two Ga–O bonds form between the adatoms, and two Ga–O bonds form between the O adatom and surface Ga atoms ($n_{bonds} = 4$). We thus have $n_e = 3 \times 2 + 6 \times 1 - 2 \times 4 = 4$. These four electrons are localized on the two DBs of the two Ga adatoms [as shown in the charge density isosurface in Fig. 4(b)] and occupy the surface states indicated by the two green bands in Fig. 4(d). Electrons in these states raise the formation energy, but due to the fact that the adatoms can form strong bonds, the overall effect is to lower the formation energy relative to the ideal surface (at least under Ga-rich conditions).

As the band gap and energy levels of surface states are underestimated using the PBE functional, we also checked the formation energy using the HSE functional for the surfaces with two H adatoms [Fig. 2(e)] and for the 2Ga+O surface [Fig. 4(b)]. The formation energy using HSE is 0.091 eV/Å^2 for (H–O$_{II}$)+(H–Ga) and 0.087 eV/Å^2 for 2Ga+O at $\Delta\mu_{Ga} = 0$. While the values for formation energies slightly differ, the *difference* in formation energies is the same in HSE as in PBE. This gives us confidence that *trends* obtained with the PBE functional are trustworthy and that the PBE results are reliable for analyzing the relative stability of different surface reconstructions.

C. Hydrogen-related reconstructions

Moving to higher $\Delta\mu_H$ values, additional reconstructions can be stabilized. The line at $\Delta\mu_H = -1.18$ eV in Fig. 3(c) is representative of conditions under chemical vapor deposition (CVD) growth. The reconstructions that are stable under these conditions [see also Fig. 3(b)] are the $4V_{Ga}+12H$ [Fig. 5(f)], $2V_{Ga}+2O+10H$ [Fig. 5(a)], $2V_{Ga}+O+8H$ [Fig. 5(b)], O+2H [Fig. 5(c)], and Ga+2O+H [Fig. 5(d)] surfaces and the aforementioned 2Ga+O and 4Ga+2O surfaces.

For highly O-rich conditions, surfaces with $2V_{Ga}+O+8H$ [Fig. 5(b)], $2V_{Ga}+2O+10H$ [Fig. 5(a)], and $4V_{Ga}+12H$ [Fig. 5(f)] are stable. The stability of $4V_{Ga}+12H$ is easily understood: As the four Ga atoms on the top layer form 14 bonds to six O atoms on the top layer and six O atoms in the second layer, removing four Ga atoms creates 14 DBs on 12 O atoms. However, since each Ga atom contributes three electrons, removing four Ga atoms leads to only 12 missing electrons; 12 H atoms therefore perfectly passivate the O atoms. The stability of $2V_{Ga}+2O+10H$ and $2V_{Ga}+O+8H$ can be understood by counting n_e. There are ten O–H bonds on the surface with $2V_{Ga}+2O+10H$. Two of them are formed between H and surface O atoms, which cannot accommodate electrons. There are six O–H bonds due to the two V_{Ga} and two O–H bonds that are formed between H and O adatoms, which can accommodate electrons. The bonds on $2V_{Ga}+2O+10H$ that can accommodate electrons include eight O–H bonds,

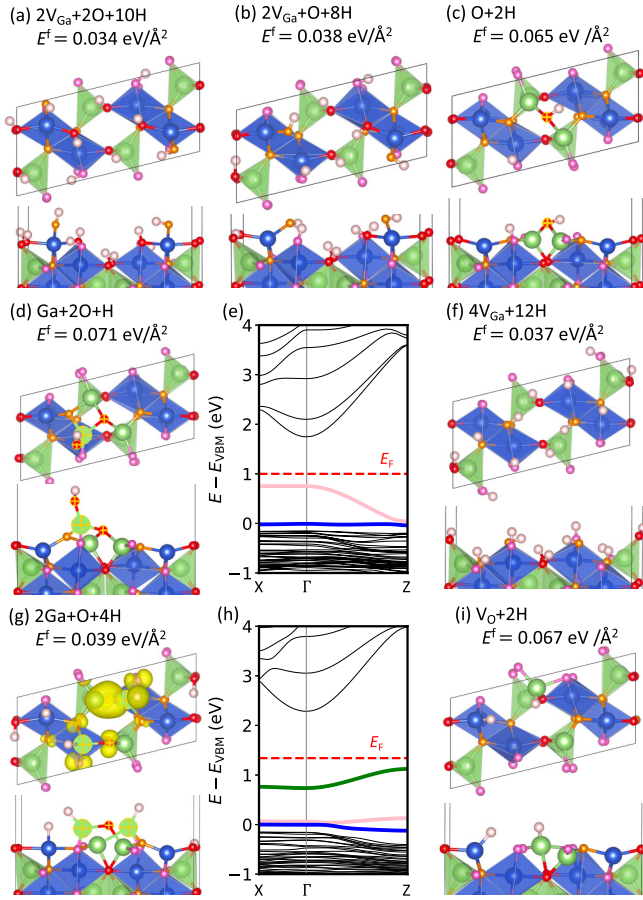FIG. 5. Structures of Ga$_2$O$_3$(010) surfaces with (a) 2V_{Ga}+2O+10H, (b) 2V_{Ga}+O+8H, (c) O+2H, (d) Ga+2O+H, (f) 4V_{Ga}+12H, (g) 2Ga+O+4H, and (i) V_O+2H reconstructions. The quoted formation energies E^f are for $\Delta\mu_{Ga} = \Delta\mu_H = 0$. Band structures of the Ga+2O+H and 2Ga+O+4H surfaces are displayed in (e) and (h). The yellow charge density isosurface superimposed on the atomic structures in (g) is for the green band. The pink bands in (e) and (h) originate from the surface states from surface O atoms.

two Ga–O bonds, and four O DBs: $n_e = 3 \times 2 + 6 \times 2 + 1 \times 10 - 2 \times 10 - 2 \times 4 = 0$. Here the $3 \times 2 = 6$ refers to the six electrons on O DBs due to the two missing Ga atoms. Similarly, on the surface with 2V_{Ga}+O+8H, there are seven O–H bonds, one Ga–O bond, and two O DBs that can accommodate electrons: $n_e = 3 \times 2 + 6 \times 1 + 1 \times 8 - 2 \times 8 - 2 \times 2 = 0$. These surfaces therefore satisfy the electron counting rule, explaining their stability.

Moving to less O-rich conditions, the surfaces with O+2H and Ga+2O+H become stable. The surface with O+2H has two Ga–O bonds, one O–H bond, and one O DB that can accommodate electrons: $n_e = 6 \times 1 + 1 \times 2 - 2 \times 3 - 2 \times 1 = 0$. The reconstruction of Ga+2O+H contains four Ga–O bonds, one O–H bond, and three O DBs, and hence $n_e = 3 \times 1 + 6 \times 2 + 1 \times 1 - 2 \times 5 - 2 \times 3 = 0$. Both surfaces fulfill electron counting. We show the band structure of the Ga+2O+H surface in Fig. 5(e); it contains no surface states related to Ga atoms, explaining the stability of this reconstruction.

Under more Ga-rich conditions ($\Delta\mu_{Ga} > -0.9$ eV), we find that the surface prefers 2Ga+O and 4Ga+2O reconstructions that do not involve any hydrogen atoms. We find that under Ga-rich conditions, hydrogen-containing surface reconstructions are stable only for very high H chemical potentials. In addition to the aforementioned O+2H and Ga+2O+H reconstructions, we find a 2Ga+O+4H reconstruction [Fig. 5(g)]. It contains two Ga–O bonds and three Ga–H bonds ($n_{bonds} = 5$); in addition, there are two O DBs ($n_{ODB} = 2$) that can accommodate electrons, and hence $n_e = 3 \times 2 + 6 \times 1 + 4 - 2 \times 5 - 2 \times 2 = 2$, explaining the stability. Compared with the surface with 2Ga+O [Fig. 4(b)], the coordination of Ga and O adatoms is changed due to the adsorption of H. For example, the O adatom is coordinated with four Ga atoms in 2Ga+O [Fig. 4(b)] and only bonded to two Ga atoms on the surface with 2Ga+O+4H [Fig. 5(g)]. The 2Ga+O+4H reconstruction has one (Ga–Ga)-related surface state in the band gap [green band in Fig. 5(h)], as opposed to two surface states for the 2Ga+O reconstruction [Fig. 4(d)]. Overall, the 2Ga+O+4H surface is stable only under highly Ga-rich and H-rich conditions [Fig. 3(c)].

It is striking that at a fixed μ_H value, H-containing reconstructions are much more prevalent under anion-rich conditions than under cation-rich conditions. This is actually similar to what was found on GaN surfaces [26], and it ultimately boils down to Ga–H bonds being significantly weaker than O–H (or N–H) bonds. To explore this, we investigated the surface with an O vacancy and two H adatoms (V_O+2H) [Fig. 5(i)]. Under O-rich conditions, the 4V_{Ga}+12H and 2V_{Ga}+O+8H surfaces are quite stable; so we might expect that under Ga-rich conditions, surfaces with oxygen vacancies would be stable. For V_O+2H, removing an O$_{III}$ atom leads to the lowest energy. Adding H adatoms to a Ga$_{octa}$ atom and a Ga$_{tetra}$ atom allows two Ga–H bonds to be formed. Still, the resulting formation energy of V_O+2H is very high [Fig. 3(a)]. Similarly, surfaces with Ga adatoms might be expected to be stable under Ga-rich conditions, but as seen with the example of the Ga+3H surface [Fig. 3(a)] this is also not competitive. The surface with Ga+3H contains three Ga–H bonds and satisfies the electron counting rule: $n_e = 3 \times 1 + 3 \times 1 - 2 \times 3 = 0$. The fact that the O–H bond is much stronger than the Ga–H bond is clearly responsible: The diatomic bond dissociation energy is 4.46 eV for an O–H bond and 2.76 eV for a Ga–H bond [32]. Hydrogen adsorption is therefore more favorable under O-rich conditions.

We finish this discussion of the (010) surface by pointing out the stability of the Ga+2O+H structure [Fig. 5(d)] over a remarkably large range of chemical potentials [Fig. 3(c)]. This range covers the conditions that are most likely to be present during MOCVD growth [see the dashed line at $\Delta\mu_H = -1.18$ eV in Fig. 3(c)]. However, we observe that this reconstruction continues to be favorable down to very low hydrogen chemical potentials, particularly under O-rich conditions. This implies that even in an ultrahigh-vacuum (UHV) environment, such as in molecular beam epitaxy (MBE), the β-Ga$_2$O$_3$(010) surface may be hydrogenated. Indeed, hydrogen is unavoidably present even in a UHV system [33,34]. Even if the residual hydrogen pressure is as low as 10^{-10} Torr, the hydrogen chemical potential at a typical MBE growth temperature of 973 K would still be -1.92 eV [Fig. 3(c)].
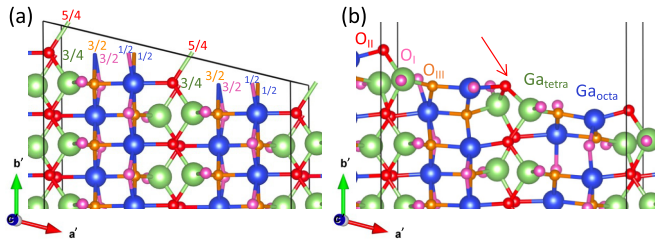
FIG. 6. (a) Electron counting on the unreconstructed and unrelaxed (110) surface. (b) Structure of the relaxed (110) surface. See Fig. 1 for the definition of the lattice vectors. The oxygen atom indicated by the red arrow in (b) undergoes a large lattice relaxation.

Figure 3(c) shows that the hydrogenated surface would prevail under those conditions, unless the Ga chemical potential is pushed to higher values (which is difficult to achieve while maintaining high-quality growth). Conversely, the present results also show that observing pristine (unhydrogenated) reconstructions of β-Ga$_2$O$_3$(010) may, in practice, be impossible, since it would require either unattainably low hydrogen chemical potential values or higher values of the gallium chemical potential that do not result in stable growth.

D. Reconstructions on the (110) surface

Alema *et al.* [9] reported that using water as the precursor instead of O$_2$ during the MOCVD growth of Ga$_2$O$_3$(010) resulted in more {110} facets, suggesting that H could potentially play a role in stabilizing the {110} facets. This motivated us to study H-related reconstructions on the Ga$_2$O$_3$(110) surface.

The Ga$_2$O$_3$(110) surface is created by breaking four Ga$_{tetra}$–O bonds and eight Ga$_{octa}$–O bonds in a 1×1 unit cell [Fig. 6(b)], resulting in two O$_I$ dangling bonds (DBs) (magenta), two O$_{II}$ DBs (red), two O$_{III}$ DBs (orange), two Ga$_{tetra}$ DBs (green), and four Ga$_{octa}$ DBs (blue). In each Ga$_{tetra}$–O bond, the Ga atom contributes 3/4 electrons, and the O atom contributes 5/4 electrons. When the bond breaks, the Ga$_{tetra}$ DB will therefore contain 3/4 electrons, while the O$_{II}$ DB will contain 5/4 electrons before any charge transfer takes place. The two electrons in a Ga$_{octa}$–O bond result from the Ga atom contributing 1/2 electrons and the O atom contributing 3/2 electrons: The resulting Ga$_{octa}$ DB contains 1/2 electrons, and each O$_I$ or O$_{III}$ DB contains 3/2 electrons before any charge transfer. The total number of electrons on the ideal Ga$_2$O$_3$(110) surface can be calculated by counting the electrons provided by the broken bonds in Fig. 6(c): The four Ga atoms provide $2 \times (3/4) + 4 \times (1/2) = 7/2$ electrons, and the six O atoms provide $2 \times (5/4) + 2 \times (3/2) + 2 \times (3/2) = 17/2$ electrons. These 12 electrons can fill all the O DBs on the Ga$_2$O$_3$(110) surface: All Ga DBs are empty and all O DBs are filled with two electrons after the electrons are transferred from Ga DBs to O DBs; therefore the electron counting rule is obeyed.

Figure 6(b) shows the relaxed structure of the (110) surface. The O atom indicated by the red arrow in Fig. 6(b) was bonded to one Ga$_{tetra}$ and one Ga$_{octa}$ on the unrelaxed surface; after relaxation, this O atom is bonded to *two* Ga$_{tetra}$ and one Ga$_{octa}$, resulting in one fewer Ga DB and one fewer
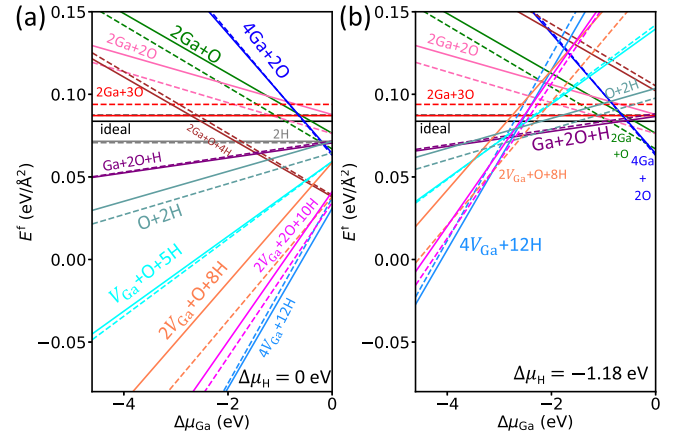

FIG. 7. Formation energies E^f (in eV/Å^2) of surface reconstructions on the Ga$_2$O$_3$(110) surface (solid lines) as a function of the Ga chemical potential when (a) $\Delta\mu_H = 0$ eV and (b) $\Delta\mu_H = -1.18$ eV. Results for the (010) surface (dashed lines) are included for comparison.

O DB compared with the ideal (010) surface. This oxygen coordination is different from the (010) surface and is evidence of a large atomic relaxation on the (110) surface. The large relaxation probably explains why the (110) surface has a slightly lower surface energy (0.085 eV/Å^2) than the (010) surface (0.087 eV/Å^2; 1 eV/Å^2 = 16.02 J/m^2), in spite of having the same number of O and Ga atoms and very similar surface areas [71.26 Å^2 for (010) and 73.54 Å^2 for (110)].

Figure 7 shows the formation energies for the ideal and reconstructed (110) surfaces. Because of the similarity in bonding compared with the (010) surface, it is not surprising that the same reconstructions turn out to be favorable. The corresponding formation energies do show some differences. Under H-poor conditions (such as when a O$_2$ precursor is used [9]), the ideal surface, the 2Ga+O reconstruction, and the 4Ga+2O reconstruction are likely to occur, with the 2Ga+O reconstruction clearly lower in energy for (010). In the presence of hydrogen (such as when an H$_2$O precursor is used [9]), the Ga+2O+H reconstruction [Fig. 8(a)] and 4V_{Ga}+12H [Fig. 8(c)] are likely to occur. The surface energies of these two structures are slightly lower for the (110) surface orientation. We also found the surface with 2Ga+O+4H [Fig. 8(b)] to be slightly lower in energy on the (110) surface. Overall, the lowering in formation energy for the hydrogenated surface of
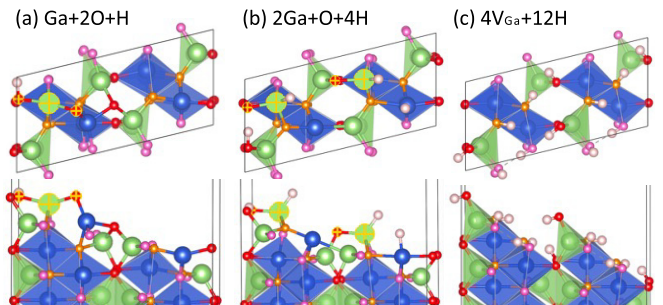

FIG. 8. Structures of the Ga$_2$O$_3$(110) surface with (a) Ga+2O+H, (b) 2Ga+O+4H, and (c) 4V_{Ga}+12H reconstructions.

(110) compared with that of (100) is quite small and may not be sufficient to explain the stabilization of {110} facets. As noted in Ref. [9], the mechanism by which use of the H_2O precursor favors {110} facet formation is probably complex and may also involve kinetics.

IV. CONCLUSION

In conclusion, we used density functional theory to investigate surface reconstructions on bare $Ga_2O_3(010)$ surfaces as well as the adsorption of hydrogen, including pure H adsorption on the ideal surface and coadsorption of Ga, O, and H under epitaxial growth conditions. We constructed a phase diagram to show surface reconstructions under different Ga and H chemical potentials.

We found that it may be difficult to observe reconstructions on the bare surface, since it would require very Ga-rich conditions. Under more O-rich conditions, hydrogenated surfaces are more stable. These results also apply to MBE growth, where hydrogen is unavoidably present as a residual gas. In order to suppress suboxide (Ga_2O) formation and etching [35], MBE growth cannot be too metal-rich, which means that hydrogen will likely be present on the surface in a Ga+2O+H reconstruction [see Fig. 3(c)], enhancing the prospect that it would be incorporated. This could actually have a beneficial impact on materials quality, since hydrogen can passivate native defects [6,7] or unintentional impurities such as carbon [30].

The Ga+2O+H reconstruction is stable over a remarkably large range of chemical potentials [Fig. 3(c)], including conditions that are most likely to be present during MOCVD growth [dashed line at $\Delta\mu_H = -1.18$ eV in Fig. 3(c)]. We suggest that the relative simplicity of this structure [Fig. 5(d)], along with the O+2H reconstruction [Fig. 5(c)], which occurs under slightly more hydrogen-rich or oxygen-rich conditions, would be conducive to growth of high-quality material, as opposed to the presence of more complex reconstructions such as $2V_{Ga}$+O+8H [Fig. 5(b)], $2V_{Ga}$+2O+10H [Fig. 5(a)], or $4V_{Ga}$+12H [Fig. 5(f)].

Due to the similarity in bonding on the ideal (110) surface compared with the (010) surface, the reconstructions on the (110) surface are the same as those on (010) with similar formation energies. Knowledge of these surface reconstructions will hopefully help in designing growth conditions that achieve optimal materials quality.

[1] K. Konishi, K. Goto, H. Murakami, Y. Kumagai, A. Kuramata, S. Yamakoshi, and M. Higashiwaki, Appl. Phys. Lett. **110**, 103506 (2017).

[2] M. Higashiwaki, K. Sasaki, A. Kuramata, T. Masui, and S. Yamakoshi, Appl. Phys. Lett. **100**, 013504 (2012).

[3] W. S. Hwang, A. Verma, H. Peelaers, V. Protasenko, S. Rouvimov, H. Xing, A. Seabaugh, W. Haensch, C. G. Van de Walle, Z. Galazka, M. Albrecht, R. Fornari, and D. Jena, Appl. Phys. Lett. **104**, 203111 (2014).

[4] J. B. Varley, J. R. Weber, A. Janotti, and C. G. Van de Walle, Appl. Phys. Lett. **97**, 142106 (2010).

[5] J. R. Ritter, J. Huso, P. T. Dickens, J. B. Varley, K. G. Lynn, and M. D. McCluskey, Appl. Phys. Lett. **113**, 052101 (2018).

[6] J. B. Varley, H. Peelaers, A. Janotti, and C. G. Van de Walle, J. Phys.: Condens. Matter **23**, 334212 (2011).

[7] Y. K. Frodason, C. Zimmermann, E. F. Verhoeven, P. M. Weiser, L. Vines, and J. B. Varley, Phys. Rev. Mater. **5**, 025402 (2021).

[8] A. Anhar Uddin Bhuiyan, Z. Feng, J. M. Johnson, Z. Chen, H.-L. Huang, J. Hwang, and H. Zhao, Appl. Phys. Lett. **115**, 120602 (2019).

[9] F. Alema, Y. Zhang, A. Mauze, T. Itoh, J. S. Speck, B. Hertog, and A. Osinsky, AIP Adv. **10**, 085002 (2020).

[10] K. Konishi, K. Goto, R. Togashi, H. Murakami, M. Higashiwaki, A. Kuramata, S. Yamakoshi, B. Monemar, and Y. Kumagai, J. Cryst. Growth **492**, 39 (2018).

[11] Z.-N. Xiong, X. Xiang-Qian, L. Yue-Wen, H. Xue-Mei, X. Zi-Li, C. Peng, L. Bin, H. Ping, R. Zhang, and Y.-D. Zheng, Chin. Phys. Lett. **35**, 058101 (2018).

[12] J. Leach, K. Udwary, T. Schneider, J. Blevins, K. Evans, G. Foundos, and K. Stevens, in *2017 CS MANTECH Conference, Indian Wells, CA, USA* (CS MANTECH, Beaverton, OR, 2017), p. 14.3.

[13] K. Goto, K. Ikenaga, N. Tanaka, M. Ishikawa, H. Machida, and Y. Kumagai, Jpn. J. Appl. Phys. **60**, 045505 (2021).

[14] M. Bosi, P. Mazzolini, L. Seravalli, and R. Fornari, J. Mater. Chem. C **8**, 10975 (2020).

[15] G. Wagner, M. Baldini, D. Gogova, M. Schmidbauer, R. Schewski, M. Albrecht, Z. Galazka, D. Klimm, and R. Fornari, Phys. Status Solidi A **211**, 27 (2014).

[16] Y.-x. Pan, D. Mei, C.-j. Liu, and Q. Ge, J. Phys. Chem. C **115**, 10140 (2011).

[17] E. A. Gonzalez, P. V. Jasen, A. Juan, S. E. Collins, M. A. Baltanás, and A. L. Bonivardi, Surf. Sci. **575**, 171 (2005).

[18] M. A. Mastro, C. R. Eddy Jr, M. J. Tadjer, J. K. Hite, J. Kim, and S. J. Pearton, J. Vac. Sci. Technol. A **39**, 013408 (2021).

[19] Y. Hinuma, T. Kamachi, N. Hamamoto, M. Takao, T. Toyao, and K.-i. Shimizu, J. Phys. Chem. C **124**, 10509 (2020).

[20] P. Mazzolini, A. Falkenstein, C. Wouters, R. Schewski, T. Markurt, Z. Galazka, M. Martin, M. Albrecht, and O. Bierwagen, APL Mater. **8**, 011107 (2020).

[21] G. Kresse and J. Furthmüller, Phys. Rev. B **54**, 11169 (1996).

[22] G. Kresse and J. Furthmüller, Comput. Mater. Sci. **6**, 15 (1996).

[23] J. P. Perdew, K. Burke, and M. Ernzerhof, Phys. Rev. Lett. **77**, 3865 (1996).

[24] J. Åhman, G. Svensson, and J. Albertsson, Acta Crystallogr. C: Cryst. Struct. Commun. **52**, 1336 (1996).

[25] M. Wang, S. Mu, and C. G. Van de Walle, Phys. Rev. B **102**, 035303 (2020).

[26] C. G. Van de Walle and J. Neugebauer, Phys. Rev. Lett. **88**, 066103 (2002).

[27] C. G. Van de Walle and J. Neugebauer, J. Vac. Sci. Technol. B **20**, 1640 (2002).

[28] J. Heyd, G. E. Scuseria, and M. Ernzerhof, J. Chem. Phys. **118**, 8207 (2003).

[29] H. J. S. Ge and M. Ernzerhof, J. Chem. Phys. **124**, 219906 (2006).

[30] S. Mu, M. Wang, J. B. Varley, J. L. Lyons, D. Wickramaratne, and C. G. Van de Walle, Phys. Rev. B **105**, 155201 (2022).

[31] M. D. Pashley, Phys. Rev. B **40**, 10481 (1989).

[32] Y.-R. Luo, *Comprehensive Handbook of Chemical Bond Energies* (CRC, Boca Raton, FL, 2007).

[33] J. E. Northrup and J. Neugebauer, Appl. Phys. Lett. **85**, 3429 (2004).

[34] C. S. Gallinat, G. Koblmüller, and J. S. Speck, Appl. Phys. Lett. **95**, 022103 (2009).

[35] P. Vogt, O. Brandt, H. Riechert, J. Lähnemann, and O. Bierwagen, Phys. Rev. Lett. **119**, 196001 (2017).